

Entanglement growth and information capacity in a quasiperiodic system with a single-particle mobility edge

Yuqi Qing,^{1,2} Yu-Qin Chen,^{3,*} and Shi-Xin Zhang^{1,†}

¹*Institute of Physics, Chinese Academy of Sciences, Beijing 100190, China*

²*Tsung-Dao Lee Institute, Shanghai Jiao Tong University, Shanghai 201210, China*

³*Graduate School of China Academy of Engineering Physics, Beijing 100193, China*

(Dated: June 24, 2025)

We investigate the quantum dynamics of a one-dimensional quasiperiodic system featuring a single-particle mobility edge (SPME), described by the generalized Aubry-André (GAA) model. This model offers a unique platform to study the consequences of coexisting localized and extended eigenstates, which contrasts sharply with the abrupt localization transition in the standard Aubry-André model. We analyze the system's response to a quantum quench through two complementary probes: entanglement entropy (EE) and subsystem information capacity (SIC). We find that the SPME induces a smooth crossover in all dynamical signatures. The EE saturation value exhibits a persistent volume-law scaling in the mobility-edge phase, with an entropy density that continuously decreases as the number of available extended states decreases. Complementing this, the SIC profile interpolates between the linear ramp characteristic of extended systems and the information trapping behavior of localized ones, directly visualizing the mixed nature of the underlying spectrum. Our results establish unambiguous dynamical fingerprints of a mobility edge, providing a crucial non-interacting benchmark for understanding information and entanglement dynamics in more complex systems with mixed phases.

Introduction.— Understanding thermalization and its breakdown in isolated quantum systems is a fundamental problem in quantum many-body physics [1, 2]. While generic interacting systems typically thermalize following the eigenstate thermalization hypothesis [3–5], this behavior can be subverted by strong quenched disorder. For example, quenched disorder can cause Anderson localization in non-interacting systems [6] and many-body localization (MBL) can emerge when interaction is turned on, leading to a nonergodic phase where memory of the initial state persists [7–10].

Besides random disorder, quasiperiodic potentials offer an alternative path to localization [11–20]. The standard Aubry-André (AA) model, for instance, shows a sharp transition where all single-particle states become localized at the critical potential strength [21, 22]. A more intriguing scenario is presented by the generalized Aubry-André (GAA) model [23–26], which holds a more complex spectral structure with a single-particle mobility edge (SPME)—an energy threshold separating coexisting localized and extended eigenstates. The recent experimental realization of such models in ultracold atoms [27] and photonic lattices [28, 29] have provided excellent platforms for theoretical study. Understanding the precise dynamical signatures in the non-interacting setting with SPME is a critical first step, providing an essential baseline for tackling the more complex and debated questions of thermalization in interacting systems that may host a mobility edge [30–35].

Concepts from quantum information theory offer powerful tools for probing quantum many-body systems [10,

36, 37]. Among these, entanglement entropy (EE) is a primary probe of correlations and quantum phase structures. The scaling of EE with subsystem size clearly separates different quantum phases, for example, ground states of gapped systems follow an area law. In terms of time-evolved states, Anderson localization systems follow an area law, while thermalizing systems follow a volume law [38, 39]. Beyond its late-time saturation value, the initial growth of entanglement entropy (EE) after a quantum quench serves as a powerful dynamical probe. Linear growth is a hallmark of chaotic thermalizing systems, logarithmic growth is characteristic of many-body localization (MBL), and a near-complete lack of growth signifies Anderson localization [40–42]. This raises a key question for the GAA model: How does entanglement evolve in a system defined by the coexistence of localized and extended modes? Does it obey a volume law due to the extended states, an area law governed by the localized ones, or does a new, intermediate behavior emerge?

While EE quantifies the overall magnitude of entanglement, it does not fully resolve how quantum information propagates and where it is stored. Other tools reveal different aspects of information dynamics. For example, mutual information tracks shared correlations [43], and its extensions like tripartite mutual information can detect delocalized entanglement and information scrambling [44]. Moreover, out-of-time-ordered correlators are frequently used to diagnose the spreading of local information into non-local correlations—a signature of quantum chaos [45–47]. However, to obtain a more direct, spatially resolved picture of how information propagates and is retained in space-time, we employ the subsystem information capacity the subsystem information capacity (SIC) [48], a recently introduced probe of information propagation and retention. This quantity investigates the

* yqchen@gscap.ac.cn

† shixinzhang@iphy.ac.cn

information flow by viewing a subsystem's evolution as an effective quantum channel whose capacity is shaped by the system's overall dynamics [49]. Defined as the mutual information $I(A:R)$ between an output subsystem A and a reference system R initially entangled with an input region E , SIC measures how much of the initial quantum information can be recovered from A after some time. This measure is closely related to the quantum coherent information of the effective channel $\mathcal{E}_{E \rightarrow A}$ [48, 50], reflecting the system's ability to preserve quantum information and acting as a measure of the channel's single-shot quantum capacity [51, 52]. Importantly, SIC shows distinct spatial profiles in different dynamical phases—from information trapping behavior in localized systems to linear growth in extended ones [48]. This makes SIC an ideal diagnostic for the mixed dynamics expected in the GAA model, allowing us to ask whether the contributions of localized and extended modes can be spatially separated.

In this work, we employ two complementary quantum information probes—entanglement entropy and subsystem information capacity—to conduct a comprehensive analysis of the quench dynamics in the non-interacting generalized Aubry-André (GAA) model. By contrasting its behavior with the abrupt localization transition in the standard AA model, we establish clear and unambiguous dynamical fingerprints of an SPME. We find that the SPME induces a crossover in both dynamical signatures, replacing the sharp transition. Specifically, the EE saturation value exhibits a persistent volume-law scaling, yet with a continuously tunable entropy density controlled by the number of available extended states. Complementing this, the SIC profile directly visualizes the mixed spectral nature, interpolating between the linear ramp characteristic of extended systems and the information trapping of localized ones. Our results provide a definitive non-interacting benchmark crucial for understanding information and entanglement dynamics in interacting systems with mixed phases.

Model and Methods.— We study the dynamics of non-interacting spinless fermions on a one-dimensional lattice with open boundary conditions, described by the Generalized Aubry-André (GAA) Hamiltonian

$$H = -t \sum_{i=1}^{L-1} (c_i^\dagger c_{i+1} + \text{h.c.}) + \sum_{i=1}^L \mu_i c_i^\dagger c_i, \quad (1)$$

where c_i^\dagger (c_i) creates (annihilates) a fermion at site i , L is the system size, and t is the nearest-neighbor hopping, set to unity ($t = 1$). The on-site quasiperiodic potential is

$$\mu_i = 2\lambda \frac{\cos(2\pi b i + \phi)}{1 - a \cos(2\pi b i + \phi)}, \quad (2)$$

with λ controlling the potential strength, $b = (\sqrt{5} - 1)/2$ an irrational number, $\phi = 0$ a global phase, and a a parameter that deforms the standard Aubry-André (AA)

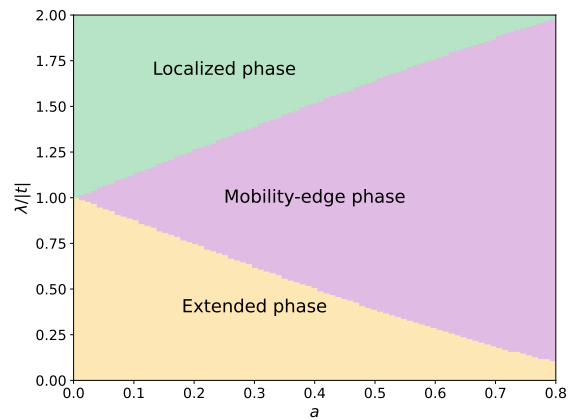


FIG. 1. Phase diagram of the GAA model, featuring three distinct dynamical regimes based on the potential strength $\lambda/|t|$ and deformation a . The model has completely extended (pink) and localized (green) phases, separated by an intermediate phase (yellow) where extended and localized states coexist due to the SPME.

model (recovered at $a = 0$). All calculations are at the half-filling sector and performed using the quantum software TensorCircuit-NG [53].

The standard AA model ($a = 0$) features a sharp localization transition at $\lambda = t$, where all single-particle eigenstates abruptly transition from being extended to localized [21]. For $a \neq 0$, the GAA model hosts a single-particle mobility edge at energy E_c , given by [26]:

$$aE_c = 2 \operatorname{sgn}(\lambda)(|t| - |\lambda|). \quad (3)$$

This critical energy leads to the phase diagram in Fig. 1, showing a completely extended, a completely localized, and an intermediate phase with a mobility edge where extended and localized states coexist.

The key feature of the GAA model for $a \neq 0$ is the coexistence of localized and extended states. The effect of the SPME is visualized by the inverse participation ratio (IPR) of the eigenstates,

$$\text{IPR}_n = \frac{\sum_{i=1}^L |\psi_{n,i}|^4}{(\sum_{i=1}^L |\psi_{n,i}|^2)^2}, \quad (4)$$

where ψ_n is the n -th eigenstate of the system. As shown in Fig. 2 for $a = 0.3$, the eigenstates are clearly separated into extended (low IPR) and localized (high IPR) modes by the energy-dependent SPME. In the following, we study the quench dynamics governed by this Hamiltonian to explore the consequences of this mixed spectral structure.

Entanglement Dynamics.— We consider unitary evolution $|\Psi(t)\rangle = e^{-iHt}|\Psi(0)\rangle$ after a quantum quench from an unentangled product state at half filling ($N = L/2$). We use the Néel state ($|1010\dots\rangle$) as the initial state throughout the main text (see SM for results from different initial states). To measure the dynamics, we com-

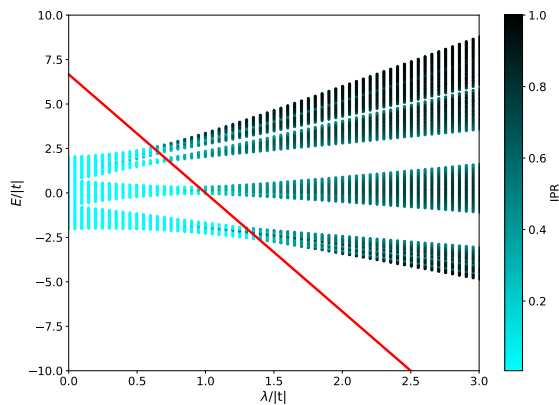


FIG. 2. Energy spectrum of the GAA model for $a = 0.3$ and $L = 200$, with eigenstates colored by their IPR. The mobility edge E_c (red lines), from Eq. (3), clearly separates extended states (low IPR, bright cyan) from localized states (high IPR, dark teal/black). This energy-dependent separation is a key feature of the SPME phase.

pute the half-chain entanglement entropy (EE), $S(t) = -\text{Tr}[\rho_{L/2}(t) \ln \rho_{L/2}(t)]$, where $\rho_{L/2}(t)$ is the reduced density matrix of the system's left half.

First, we examine the early-time EE growth velocity, v_S , extracted from the initial linear growth regime (see SM for entanglement dynamics plots). As shown in Fig. 3, for the standard AA model ($a = 0$), v_S decreases monotonically with increasing λ . For $a > 0$, the behavior is more complex: while v_S still decreases with λ , distinct plateaus appear. These plateaus are a non-trivial signature of the energy spectrum of the GAA model, appearing when the SPME aligns with the system's energy gaps (see Fig. 2). Notably, the growth speed of EE v_S begins to decrease as long as $\lambda > 0$ even in the fully extended phases. This reflects the fact that any quasiperiodic potential, no matter how weak, slows down particle propagation. This early-time character is in stark contrast to the behavior of late-time EE S_{sat} introduced next, which remains constant at fully extended phase and begins to drop at the intermediate phase.

Next, we analyze the long-time saturation EE, S_{sat} , extracted by averaging the EE over a long-time window after it reaches a steady value. As shown in Fig. 4, for the standard AA model ($a = 0$), S_{sat} drops sharply at the $\lambda = t$ transition, signaling the phase transition nature from a volume-law to an area-law phase. In contrast, the GAA models ($a > 0$) exhibit a smooth crossover, indicating a gradual suppression of entanglement generation rather than a complete halt. The visible plateaus again correspond to the SPME traversing the spectral gaps.

To rigorously probe the scaling law for the entanglement, we perform a finite-size analysis of S_{sat} (Fig. 5). The entropy density, $S_{\text{sat}}/(L/2)$, distinguishes area-law scaling ($\sim 1/L$) from volume-law scaling ($\sim \text{const}$). All cases show volume-law behavior for small λ and area-law for large λ . Importantly, in the intermediate phase with

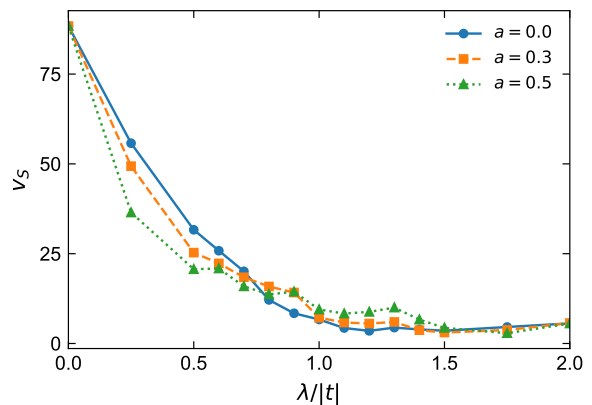


FIG. 3. Early-time EE growth velocity v_S versus $\lambda/|t|$ for different a . The initial state is a Néel state with $L = 200$. While the AA model ($a = 0$) shows a simple decrease, the GAA model ($a > 0$) exhibits plateaus. These features are signatures of the energy gaps in the SPME phase.

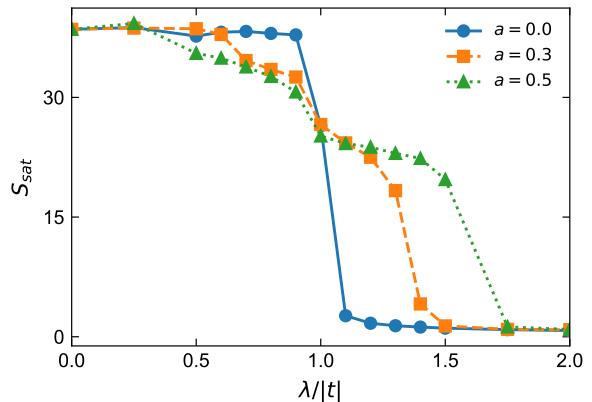


FIG. 4. Saturation EE S_{sat} versus $\lambda/|t|$ after a quench from the Néel state for $L = 200$. The AA model ($a = 0$, blue) has a sharp drop at the $\lambda = t$ transition. The GAA models ($a > 0$) show a smooth crossover, indicating partial delocalization caused by the SPME.

SPME for $a \neq 0$ (e.g., $\lambda/|t| = 1.0, 1.3$), we find a persistent volume law, with $S_{\text{sat}}/(L/2)$ approaching a nonzero constant as $L \rightarrow \infty$. This confirms that the system remains partially delocalized and capable of generating extensive entanglement throughout this phase, a defining feature absent in the standard AA model where $\lambda > t$ implies full localization and an area law.

The underlying physical mechanism is revealed in Fig. 6, which plots S_{sat} against the number of extended states, N_e (states with $|E| < |E_c|$). The two quantities are strongly correlated. This striking one-to-one correspondence demonstrates that the system's capacity to generate volume-law entanglement is directly controlled by the fraction of available extended modes, which act as resources for thermalization. In other words, the decrease in S_{sat} tracks the reduction in available extended modes as λ increases.

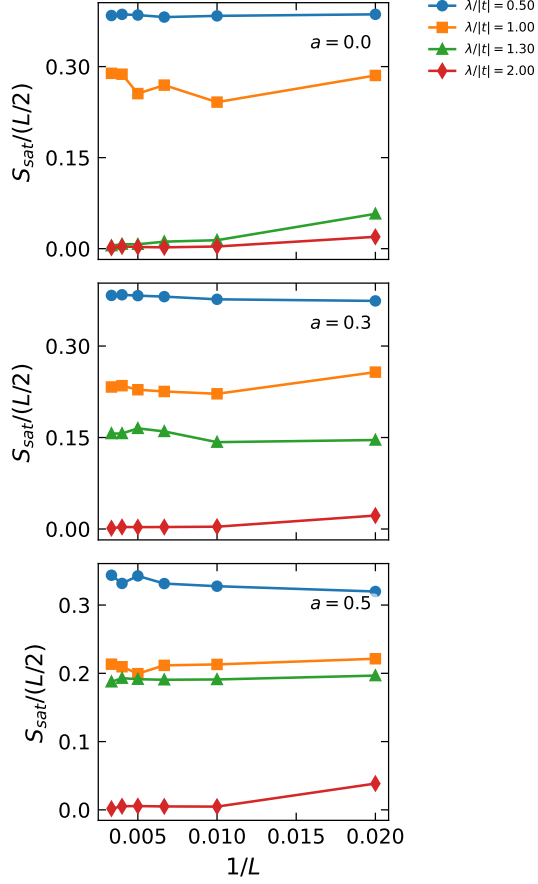


FIG. 5. Finite-size scaling of the saturation entropy density $S_{\text{sat}}/(L/2)$ versus inverse system size $1/L$. Each panel is for a different a . The data distinguishes area-law (density vanishes as $1/L \rightarrow 0$) from volume-law (density converges to a finite value) scaling. The persistent volume law for $a > 0$ at intermediate λ confirms the delocalizing effect of the SPME.

Subsystem Information Capacity.— To move beyond the single scalar value of EE and gain a spatially resolved picture of information dynamics, we analyze the SIC [48]. This probe measures how quantum information, initially localized at a single site, propagates through the system. We prepare the system with a reference qubit R maximally entangled with a single site E of the chain:

$$|\Phi\rangle = \frac{1}{\sqrt{2}}(|1\rangle_E|0\rangle_R + |0\rangle_E|1\rangle_R), \quad (5)$$

with the rest of the chain in a product state. We compute the SIC between R and a subsystem A of size $|A|$ centered on $E = L/2$ after the time evolution, defined as

$$I(A : R) = S(A) + S(R) - S(AR), \quad (6)$$

where $S(\cdot)$ is the von Neumann entropy. Note that we

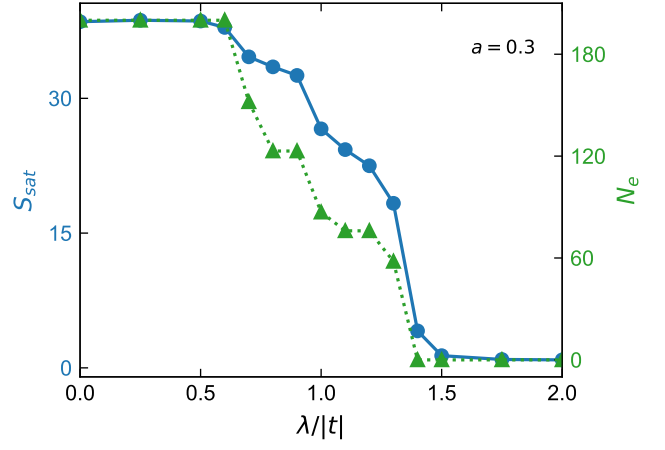


FIG. 6. Connection between saturation entanglement S_{sat} (blue circles, left axis) and the number of extended states N_e (green triangles, right axis) versus $\lambda/|t|$ for $a = 0.3$ and $L = 200$. N_e is the number of states with $|E| < |E_c|$. The strong correlation shows that the system's capability to develop volume-law entanglement is directly controlled by the number of available extended modes.

use logarithmic base 2 for the entropy convention in the SIC definition so that $I = 2$ indicates the full information recovery capability. The spatial profile of steady-state $I(A : R)$ measures how information spreads: a linear ramp signifies ballistic transport in extended systems, whereas a step-function profile indicates information trapping in localized systems [48].

The steady-state SIC profile (Fig. 7) provides a clear picture of the information distribution at late times. For the standard AA model ($a = 0$), the profile shows a sharp transition from a perfect linear ramp ($\lambda/|t| < 1$) to a sharp step function ($\lambda/|t| > 1$). In contrast, the GAA model ($a > 0$) shows a more smooth crossover. In the intermediate SPME regime, the SIC profiles are a hybrid of both behaviors: they rise steeply for small $|A|$, a signature of the localized modes trapping a portion of the information, and then continue to increase slowly for larger $|A|$, driven by the ballistic spreading through the remaining extended modes. This interpolation between a linear ramp and information trapping is a direct and powerful dynamical signature of the SPME.

To quantify the mixed behavior, we define SIC_{jump} as the SIC value for a small subsystem size (we use $|A| = 5$) intended to capture the information confined by localized modes due to the trapping nature. Fig. 8 plots SIC_{jump} and the number of localized states, N_l (states with $|E| > |E_c|$). For small λ in the fully extended phase, SIC_{jump} is near zero. As λ increases in the intermediate phase with SPME, SIC_{jump} rises sharply, tracking the increase in N_l . This powerful correlation between SIC_{jump} and the number of localized states N_l confirms the physical origin of the mixed SIC profile: the initial jump is a direct consequence of the growing fraction of localized states, which trap a corresponding amount of informa-

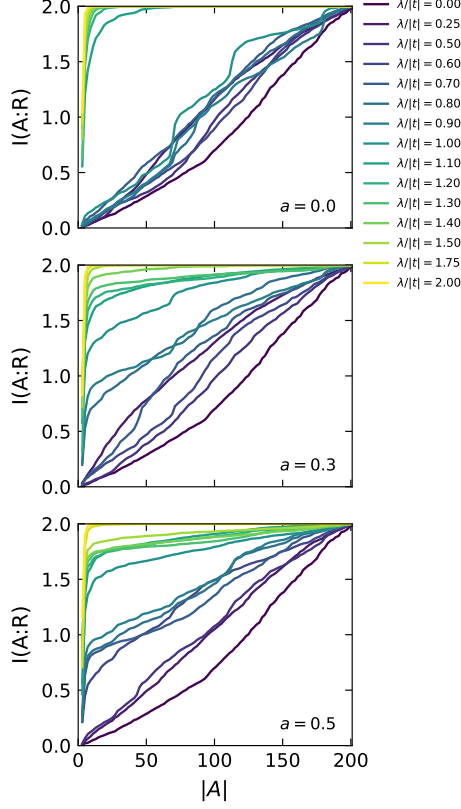


FIG. 7. Steady-state SIC profile $I(A : R)$ versus subsystem size $|A|$ for $L = 200$. The reference qubit is entangled with the center site $E = L/2$. (Top) The AA model ($a = 0$) shows a sharp transition from a linear ramp to a step function. (Middle, Bottom) The GAA model ($a > 0$) shows a smooth crossover. The hybrid nature of the profiles in the SPME phase—an initial jump followed by a slow ramp—is a direct visualization of the coexisting localized (information trapping) and extended (information spreading) modes.

tion around the initial site. We also present the late-time SIC profiles when the reference site is coupled to the boundary site in the SM, which further corroborates our findings.

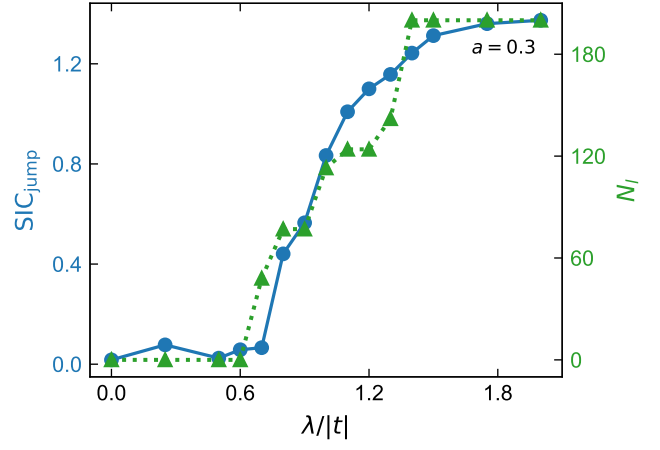


FIG. 8. Connection between the initial SIC jump, SIC_{jump} (blue circles, left axis), and the number of localized states N_l (green triangles, right axis) for the GAA model with $a = 0.3$ and $L = 200$. N_l is the number of states with $|E| > |E_c|$. The close connection shows that the emergence of information confinement, captured in SIC_{jump} , is directly caused by the increase in localized states.

TABLE I. Comparison of dynamical signatures in the standard AA and GAA models within SPME phases.

Probe	Standard AA	GAA
	($a = 0$)	($a > 0$)
EE (S_{sat})	Sharp transition:	SPME phase:
	Volume \rightarrow Area	Persistent volume-law
SIC Profile	Sharp transition:	SPME phase:
	ramp \rightarrow step-func.	Hybrid jump+ramp

Discussions and conclusion.— Our comprehensive analysis shows a clear difference between the dynamics of the standard AA model and the GAA model with an SPME. In the AA model ($a = 0$), the transition is sudden: S_{sat} switches from volume-law to area-law scaling abruptly, and the SIC profile changes from a ramp to a step. In contrast, the GAA model ($a \neq 0$) shows a smooth crossover. This is characterized by intermediate S_{sat} values, mixed SIC profiles, and a persistent volume law with a decreasing entropy density. This smoothing is a direct result of the SPME, which allows localized and extended modes to coexist and control the balance between information spreading and confinement. Our main findings are summarized in Table I. Our results provide clear, non-interacting dynamical signatures of a mobility edge, establishing an important reference for understanding thermalization in more complex quasiperiodic systems. These insights are relevant to the current debate on MBL in the presence of an SPME [30–32, 35]. While we focus on the paradigmatic GAA model, our findings on the dynamical signatures of coexisting states are expected to provide insights for other systems hosting

mobility edges, such as those with long-range interactions or in higher dimensions [17, 33, 35].

In conclusion, we have studied the quantum dynamics in the generalized Aubry-André model, a paradigmatic system with a single-particle mobility edge. By leveraging the complementary power of entanglement entropy and subsystem information capacity, we have demonstrated that the SPME fundamentally reshapes the system’s dynamical response, converting the sharp localization transition into a smooth crossover. Instead of the sudden transition in the standard AA model, the SPME facilitates a regime with smoothly varying entanglement, hybrid information-spreading profiles, and a robust volume law with tunable entropy density. Our findings highlight that these quantum information probes are highly

sensitive to a system’s spectral structure and that mobility edges reshape dynamical phase boundaries. This work provides a clear and crucial non-interacting reference for localization dynamics in quasiperiodic systems and paves the way for future studies of interacting systems, where the interplay between SPMEs and many-body effects remains a major open question. Furthermore, understanding the control over information flow offered by an SPME, from ballistic transport to perfect trapping, holds potential relevance for quantum technologies.

Acknowledgements. SXZ acknowledges the support from a start-up grant at IOP-CAS.

Data availability. Code implementation and numerical data for this manuscript are publicly accessible in Ref. [54].

-
- [1] Luca D’Alessio, Yariv Kafri, Anatoli Polkovnikov, and Marcos Rigol, “From quantum chaos and eigenstate thermalization to statistical mechanics and thermodynamics,” *Advances in Physics* **65**, 239–362 (2016).
 - [2] Joshua M Deutsch, “Eigenstate thermalization hypothesis,” *Reports on Progress in Physics* **81**, 082001 (2018).
 - [3] J. M. Deutsch, “Quantum statistical mechanics in a closed system,” *Physical Review A* **43**, 2046–2049 (1991).
 - [4] Mark Srednicki, “Chaos and quantum thermalization,” *Physical Review E* **50**, 888–901 (1994).
 - [5] Marcos Rigol, Vanja Dunjko, and Maxim Olshanii, “Thermalization and its mechanism for generic isolated quantum systems,” *Nature* **452**, 854–858 (2008).
 - [6] P. W. Anderson, “Absence of diffusion in certain random lattices,” *Physical Review* **109**, 1492–1505 (1958).
 - [7] L. Fleishman and P. W. Anderson, “Interactions and the anderson transition,” *Physical Review B* **21**, 2366–2377 (1980).
 - [8] D.M. Basko, I.L. Aleiner, and B.L. Altshuler, “Metal-insulator transition in a weakly interacting many-electron system with localized single-particle states,” *Annals of Physics* **321**, 1126–1205 (2006).
 - [9] Rahul Nandkishore and David A. Huse, “Many-body localization and thermalization in quantum statistical mechanics,” *Annual Review of Condensed Matter Physics* **6**, 15–38 (2015).
 - [10] Dmitry A. Abanin, Ehud Altman, Immanuel Bloch, and Maksym Serbyn, “Colloquium: Many-body localization, thermalization, and entanglement,” *Reviews of Modern Physics* **91**, 021001 (2019).
 - [11] Shankar Iyer, Vadim Oganesyan, Gil Refael, and David A. Huse, “Many-body localization in a quasiperiodic system,” *Physical Review B* **87**, 134202 (2013).
 - [12] Mac Lee, Thomas R Look, D N Sheng, and S P Lim, “Many-body localization in spin chain systems with quasiperiodic fields,” *Phys. Rev. B* **96**, 75146 (2017).
 - [13] Anushya Chandran and C R Laumann, “Localization and symmetry breaking in the quantum quasiperiodic ising glass,” *Phys. Rev. X* **7**, 31061 (2017).
 - [14] F Setiawan, Dong-Ling Deng, and J H Pixley, “Transport properties across the many-body localization transition in quasiperiodic and random systems,” *Phys. Rev. B* **96**, 104205 (2017).
 - [15] Michael Schreiber, Sean S. Hodgman, Pranjal Bordia, Henrik P. Lüschen, Mark H. Fischer, Ronen Vosk, Ehud Altman, Ulrich Schneider, and Immanuel Bloch, “Observation of many-body localization of interacting fermions in a quasi-random optical lattice,” *Science* **349**, 842 (2015).
 - [16] Vedika Khemani, D. N. Sheng, and David A. Huse, “Two universality classes for the many-body localization transition,” *Physical Review Letters* **119**, 075702 (2017).
 - [17] Shi-Xin Zhang and Hong Yao, “Universal properties of many-body localization transitions in quasiperiodic systems,” *Phys. Rev. Lett.* **121**, 206601 (2018).
 - [18] Shi-Xin Zhang and Hong Yao, “Strong and weak many-body localizations,” *arXiv:1906.00971* (2019).
 - [19] Yucheng Wang, Xu Xia, Long Zhang, Hepeng Yao, Shu Chen, Jiangong You, Qi Zhou, and Xiong-Jun Liu, “One-dimensional quasiperiodic mosaic lattice with exact mobility edges,” *Physical Review Letters* **125**, 196604 (2020).
 - [20] Liang-Jun Zhai, Shuai Yin, and Guang-Yao Huang, “Many-body localization in a non-hermitian quasiperiodic system,” *Physical Review B* **102**, 064206 (2020).
 - [21] Serge Aubry and Gilles André, “Analyticity breaking and anderson localization in incommensurate lattices,” *Ann. Israel Phys. Soc* **3**, 18 (1980).
 - [22] P. G. Harper, “Single band motion of conduction electrons in a uniform magnetic field,” *Proceedings of the Physical Society. Section A* **68**, 874 (1955).
 - [23] D. J. Thouless, “Quantization of particle transport,” *Physical Review B* **27**, 6083–6087 (1983).
 - [24] J. H. Han, D. J. Thouless, H. Hiramoto, and M. Kohmoto, “Critical and bicritical properties of harper’s equation with next-nearest-neighbor coupling,” *Physical Review B* **50**, 11365–11380 (1994).
 - [25] J. Biddle and S. Das Sarma, “Predicted mobility edges in one-dimensional incommensurate optical lattices: An exactly solvable model of anderson localization,” *Physical Review Letters* **104**, 070601 (2010).
 - [26] Sriram Ganeshan, J. H. Pixley, and S. Das Sarma, “Nearest neighbor tight binding models with an exact mobility edge in one dimension,” *Physical Review Letters* **114**, 146601 (2015).
 - [27] Thomas Kohlert, Sebastian Scherg, Xiao Li, Henrik P.

- Lüschen, Sankar Das Sarma, Immanuel Bloch, and Monika Aidelsburger, “Observation of many-body localization in a one-dimensional system with a single-particle mobility edge,” *Physical Review Letters* **122**, 170403 (2019).
- [28] Mor Verbin, Oded Zilberberg, Yoav Lahini, Yaacov E. Kraus, and Yaron Silberberg, “Topological pumping over a photonic fibonacci quasicrystal,” *Physical Review B* **91**, 064201 (2015).
- [29] Henrik P. Lüschen, Sebastian Scherg, Thomas Kohlert, Michael Schreiber, Pranjali Bordia, Xiao Li, S. Das Sarma, and Immanuel Bloch, “Single-particle mobility edge in a one-dimensional quasiperiodic optical lattice,” *Physical Review Letters* **120**, 160404 (2018).
- [30] Xiaopeng Li, Sriram Ganeshan, J. H. Pixley, and S. Das Sarma, “Many-body localization and quantum nonergodicity in a model with a single-particle mobility edge,” *Physical Review Letters* **115**, 186601 (2015).
- [31] Ranjan Modak and Subroto Mukerjee, “Many-body localization in the presence of a single-particle mobility edge,” *Physical Review Letters* **115**, 230401 (2015).
- [32] Dong-Ling Deng, Sriram Ganeshan, Xiaopeng Li, Ranjan Modak, Subroto Mukerjee, and J. H. Pixley, “Many-body localization in incommensurate models with a mobility edge,” *Annalen der Physik* **529**, 1600399 (2017).
- [33] Xiaopeng Li, J. H. Pixley, Dong-Ling Deng, Sriram Ganeshan, and S. Das Sarma, “Quantum nonergodicity and fermion localization in a system with a single-particle mobility edge,” *Physical Review B* **93**, 184204 (2016).
- [34] Ranjan Modak, Soumi Ghosh, and Subroto Mukerjee, “Criterion for the occurrence of many-body localization in the presence of a single-particle mobility edge,” *Physical Review B* **97**, 104204 (2018).
- [35] Ke Huang, DinhDuy Vu, Xiao Li, and S. Das Sarma, “Incommensurate many-body localization in the presence of long-range hopping and single-particle mobility edge,” *Physical Review B* **107**, 035129 (2023).
- [36] Luigi Amico, Rosario Fazio, Andreas Osterloh, and Vlatko Vedral, “Entanglement in many-body systems,” *Reviews of Modern Physics* **80**, 517–576 (2008).
- [37] J. Eisert, M. Cramer, and M. B. Plenio, “Colloquium: Area laws for the entanglement entropy,” *Reviews of Modern Physics* **82**, 277–306 (2010).
- [38] Bela Bauer and Chetan Nayak, “Area laws in a many-body localized state and its implications for topological order,” *Journal of Statistical Mechanics: Theory and Experiment* **2013**, P09005 (2013).
- [39] Adam M. Kaufman, M. Eric Tai, Alexander Lukin, Matthew Rispoli, Robert Schittko, Philipp M. Preiss, and Markus Greiner, “Quantum thermalization through entanglement in an isolated many-body system,” *Science* **353**, 794–800 (2016).
- [40] Jens H. Bardarson, Frank Pollmann, and Joel E. Moore, “Unbounded growth of entanglement in models of many-body localization,” *Physical Review Letters* **109**, 017202 (2012).
- [41] Arun Nandori, Hyungwon Kim, and David A. Huse, “Entanglement spreading in a many-body localized system,” *Physical Review B* **90**, 064201 (2014).
- [42] R. J. Lewis-Swan, A. Safavi-Naini, A. M. Kaufman, and A. M. Rey, “Dynamics of quantum information,” *Nature Reviews Physics* **1**, 627–634 (2019).
- [43] Michael M. Wolf, Frank Verstraete, Matthew B. Hastings, and J. Ignacio Cirac, “Area laws in quantum systems: Mutual information and correlations,” *Physical Review Letters* **100**, 070502 (2008).
- [44] Pavan Hosur, Xiao-Liang Qi, Daniel A. Roberts, and Beni Yoshida, “Chaos in quantum channels,” *Journal of High Energy Physics* **2016**, 4 (2016).
- [45] Juan Maldacena, Stephen H. Shenker, and Douglas Stanford, “A bound on chaos,” *Journal of High Energy Physics* **2016**, 106 (2016).
- [46] Ruihua Fan, Pengfei Zhang, Huitao Shen, and Hui Zhai, “Out-of-time-order correlation for many-body localization,” *Science Bulletin* **62**, 707–711 (2017).
- [47] Adam Nahum, Sagar Vijay, and Jeongwan Haah, “Operator spreading in random unitary circuits,” *Physical Review X* **8**, 021014 (2018).
- [48] Yu-Qin Chen, Shuo Liu, and Shi-Xin Zhang, “Subsystem information capacity in random circuits and hamiltonian dynamics,” (2024), arXiv:2405.05076 [quant-ph].
- [49] Alexander S. Holevo, *Quantum Systems, Channels, Information: A Mathematical Introduction* (De Gruyter, 2012).
- [50] Benjamin Schumacher and M. A. Nielsen, “Quantum data processing and error correction,” *Physical Review A* **54**, 2629–2635 (1996).
- [51] Seth Lloyd, “Capacity of the noisy quantum channel,” *Physical Review A* **55**, 1613–1622 (1997).
- [52] Igor Devetak and Andreas Winter, “Distillation of secret key and entanglement from quantum states,” *Proceedings of the Royal Society A: Mathematical, Physical and Engineering Sciences* **461**, 207–235 (2005).
- [53] Shi-Xin Zhang, Jonathan Allcock, Zhou-Quan Wan, Shuo Liu, Jiaze Sun, Hao Yu, Xing-Han Yang, Jiezhong Qiu, Zhao Feng Ye, Yu-Qin Chen, Chee-Kong Lee, Yi-Cong Zheng, Shao-Kai Jian, Hong Yao, Chang-Yu Hsieh, and Shengyu Zhang, “TensorCircuit: a Quantum Software Framework for the NISQ Era,” *Quantum* **7**, 912 (2023). <https://github.com/tensorcircuit/tensorcircuit-ng>.
- [54] https://gitee.com/yuqiying/sic_in_gaa_model.

Supplemental Material for "Entanglement growth and information capacity in a quasiperiodic system with a single-particle mobility edge"

CONTENTS

I. Time evolution for entanglement entropy	8
II. Entanglement growth from other initial states	8
III. Steady-state SIC profile for edge-coupling and other initial states	9

I. TIME EVOLUTION FOR ENTANGLEMENT ENTROPY

In this section, we provide details on the extraction of the early-time entanglement growth velocity v_S and the late-time saturation value S_{sat} from the time evolution of the half-chain entanglement entropy (EE). Figure S1 shows the time evolution of EE for a quench from the Néel state. The dynamics can be separated into two distinct regimes:

1. **Early-time linear growth regime:** For short times after the quench, the EE grows approximately linearly. We extract the velocity v_S by performing a linear fit to the EE curve in this initial period. In practice, the time window $t \in [0, 20]$ serves as a reasonable choice to identify the early-time regime in the system under investigation.
2. **Late-time saturation regime:** At long times, the EE stops growing and oscillates around a steady-state value. We calculate the saturation value S_{sat} by averaging the EE over a long-time window in this saturation regime, after the initial growth has ceased. In our calculation, we first quench the system for a sufficiently long time $t = 10000$, and then take 1000 samples with an average time interval of $\langle dt \rangle = 10$. To ensure adequate sampling along the EE profile, the interval dt is randomly varied around the average.

The values of v_S and S_{sat} presented in the main text and this supplemental material are obtained using this procedure.

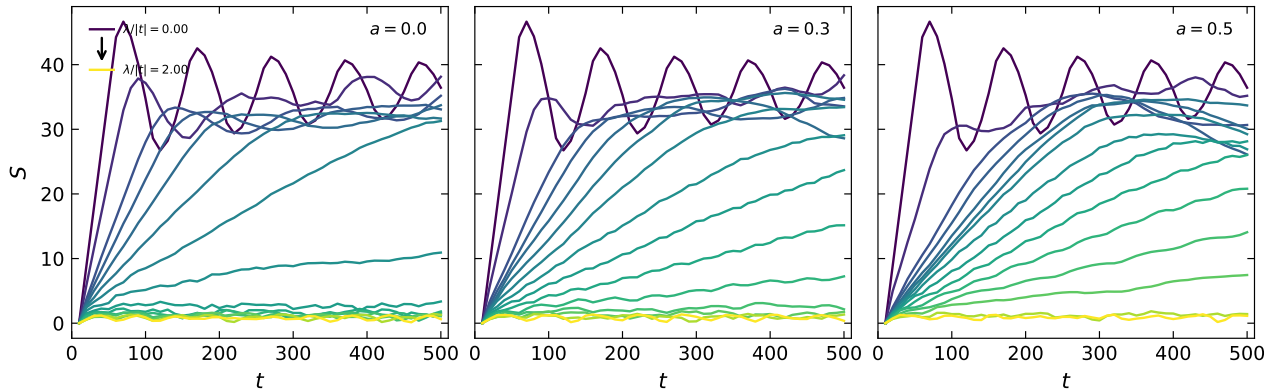


FIG. S1. Time evolution of half-chain entanglement entropy (EE) from the Néel state. The plots show EE as a function of time t for different values of the potential strength $\lambda/|t|$ (from $\lambda/|t| = 0$, top curve, to $\lambda/|t| = 2.0$, bottom curve) and deformation parameter a . The system size is $L = 200$. The dynamics clearly show an initial growth phase followed by the saturation stage.

II. ENTANGLEMENT GROWTH FROM OTHER INITIAL STATES

To ensure the generality of our conclusions, we supplement the results from the Néel state with data from two other types of initial product states at half-filling: the domain-wall state ($|11\dots 100\dots 0\rangle$) and random product states. For the random states, we average the results over different random configurations of $L/2$ fermions.

Figure S2 shows the time evolution of EE for these states. While the qualitative behavior is similar to the Néel state, we note that for the domain-wall state, the oscillation period in the saturation regime is significantly longer. The saturation values (Fig. S3) also show trends consistent with the main text: a sharp transition for the AA model ($a = 0$) and a smooth crossover for the GAA model ($a > 0$). Notably, Fig. S4 demonstrates that for both the domain-wall and random initial states, the saturation EE S_{sat} is strongly correlated with the number of extended states N_e , reinforcing the universality of our central conclusion.

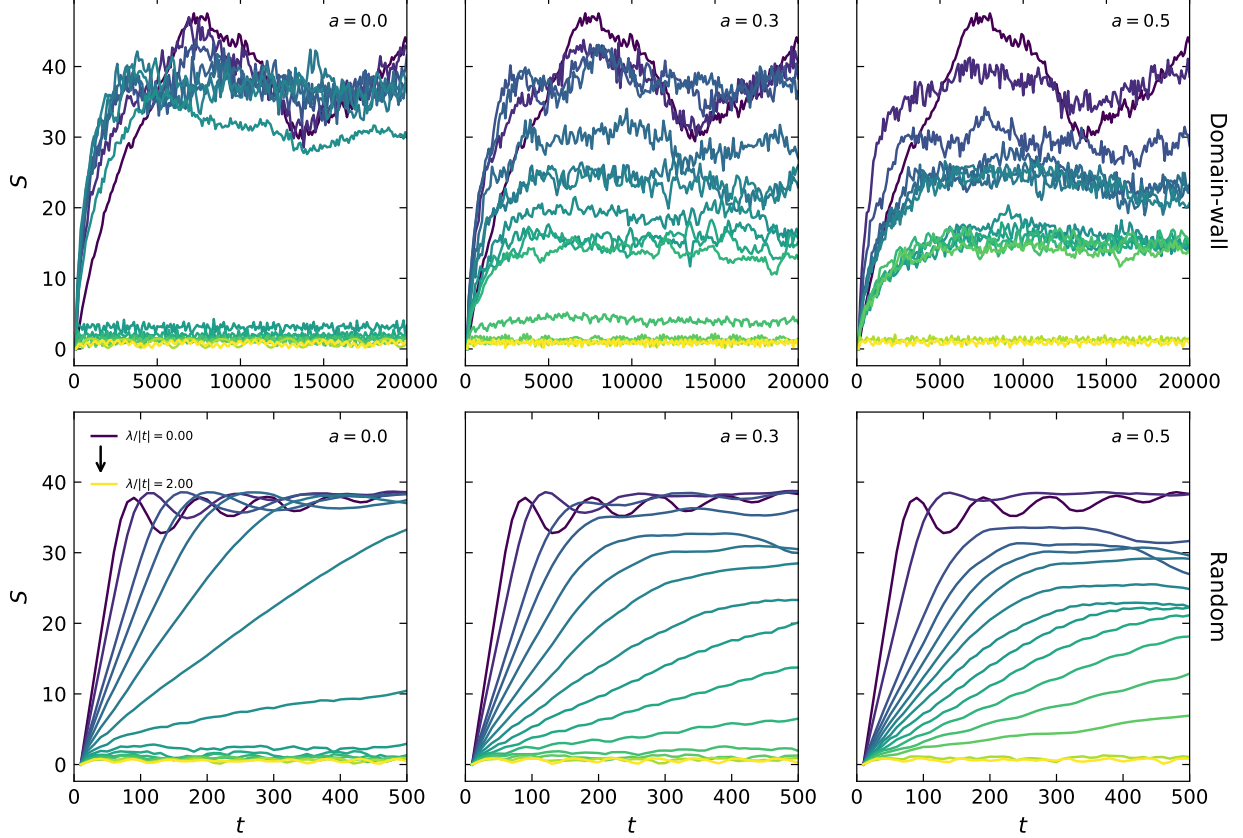


FIG. S2. Time evolution of EE for other initial states. (Top row) Quench from a domain-wall state. (Bottom row) Quench from random product states (averaged). The parameters are $L = 200$. The qualitative features of EE growth and saturation are consistent across different initial states.

III. STEADY-STATE SIC PROFILE FOR EDGE-COUPLING AND OTHER INITIAL STATES

To study boundary effects, we also investigate the steady-state SIC profile by coupling the reference site to an edge site ($E = 1$). As shown in Fig. S5, the SIC profile for this edge-coupling setup is different from the center-coupling case, especially for the standard AA model. In this case, the SIC profile fails to act as a clear probe for the phase transition, as the profile varies smoothly with increasing λ even in the extended phase. This failure might be due to the asymmetric information propagation with boundary reflections and interference.

Finally, we present the subsystem information capacity (SIC) results for different initial states mentioned before. Figures S6 and S7 show the SIC profiles for center- and edge-coupling, respectively. The results confirm that the hybrid SIC profile is a generic dynamical signature of the SPME, independent of the specific initial product state.

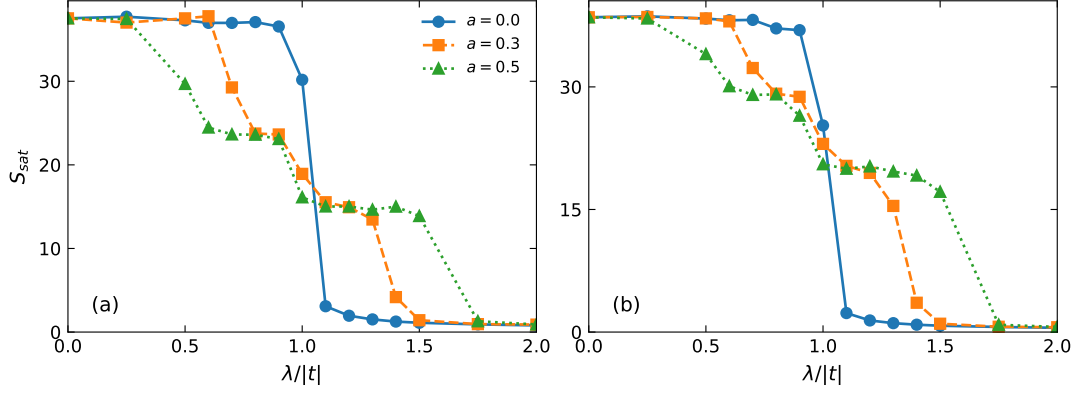


FIG. S3. Saturation EE for other initial states. (a) Domain-wall initial state. (b) Random initial states (averaged). The plots show S_{sat} versus $\lambda/|t|$. The smooth crossover in the GAA model ($a > 0$) with plateaus corresponding to the spectrum gap is a robust feature.

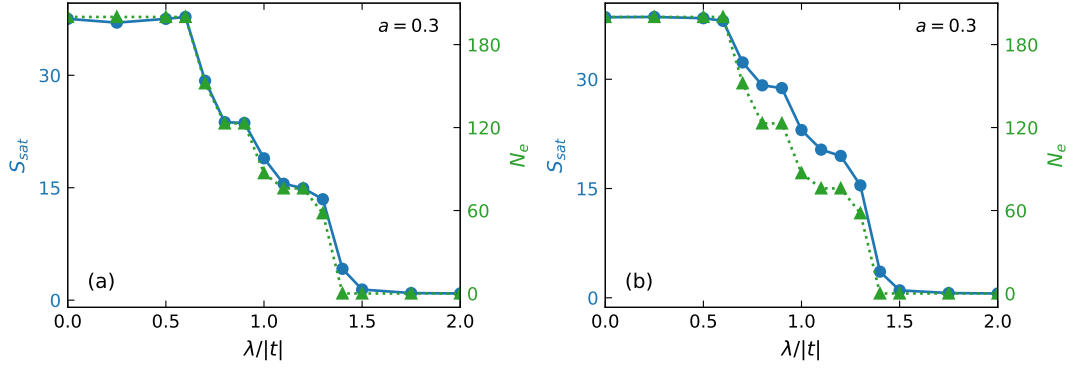


FIG. S4. Connection between saturation EE and the number of extended states for other initial states. (a) Domain-wall initial state. (b) Random initial states (averaged). Both plots are for $a = 0.3$ and $L = 200$. S_{sat} (blue circles, left axis) strongly correlates with N_e (green triangles, right axis), confirming the conclusion from the main text.

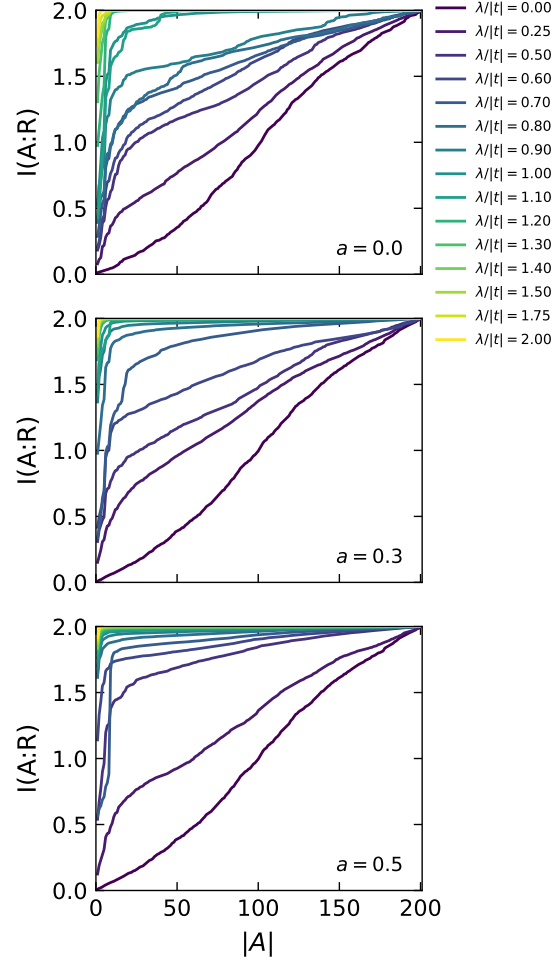


FIG. S5. Steady-state SIC profile $I(A : R)$ for the edge-coupling case. The initial state is Néel state. The reference qubit is entangled with the edge site $E = 1$, and the subsystem A starts from this edge.

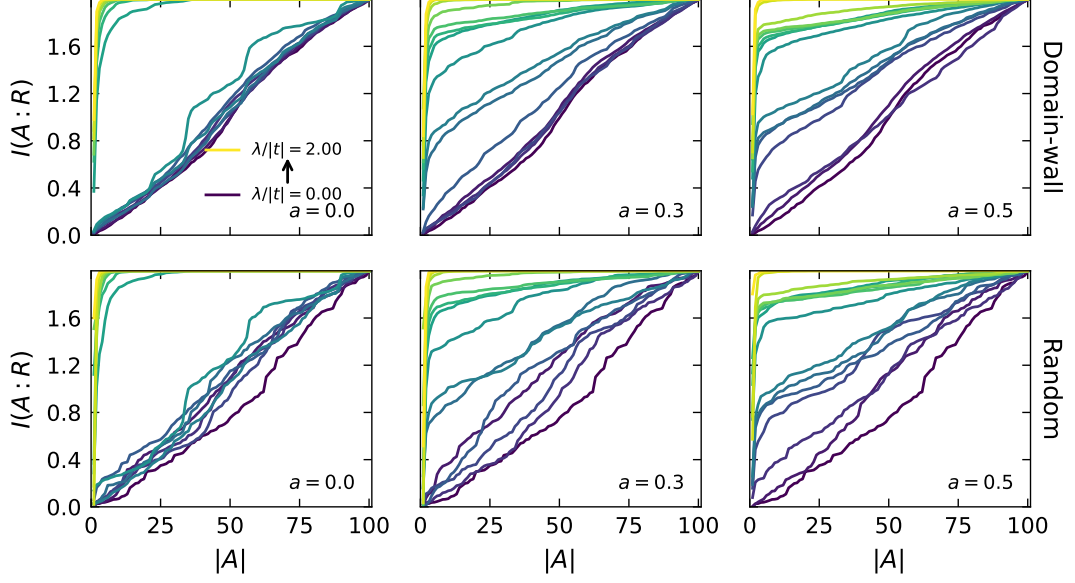


FIG. S6. SIC profiles for center-coupling with other initial states. The reference qubit is entangled with the center site $E = L/2$. (Top row) Domain-wall initial state. (Bottom row) Random initial states (averaged). System size $L = 200$, subsystem size $|A|$ is measured for the central region. The mixed SIC profile in the GAA model is a generic feature.

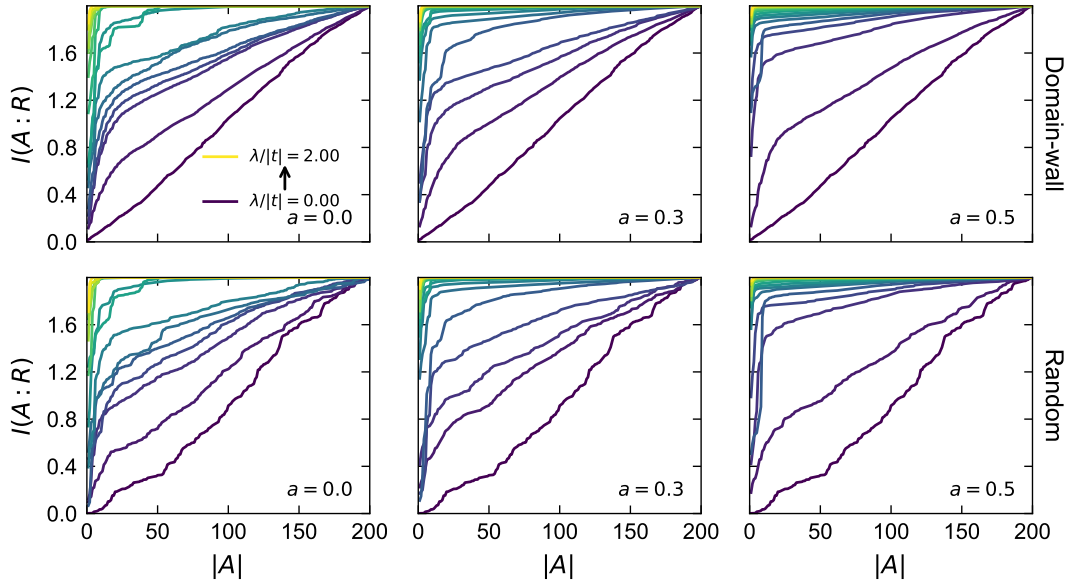


FIG. S7. SIC profiles for edge-coupling with other initial states. The reference qubit is entangled with the edge site $E = 1$. (Top row) Domain-wall initial state. (Bottom row) Random initial states (averaged). System size $L = 200$. The results are consistent with those in the main text.